

Journal of Materials Chemistry A

Accepted Manuscript



This is an *Accepted Manuscript*, which has been through the Royal Society of Chemistry peer review process and has been accepted for publication.

Accepted Manuscripts are published online shortly after acceptance, before technical editing, formatting and proof reading. Using this free service, authors can make their results available to the community, in citable form, before we publish the edited article. We will replace this *Accepted Manuscript* with the edited and formatted *Advance Article* as soon as it is available.

You can find more information about *Accepted Manuscripts* in the [Information for Authors](#).

Please note that technical editing may introduce minor changes to the text and/or graphics, which may alter content. The journal's standard [Terms & Conditions](#) and the [Ethical guidelines](#) still apply. In no event shall the Royal Society of Chemistry be held responsible for any errors or omissions in this *Accepted Manuscript* or any consequences arising from the use of any information it contains.



Journal Name

ARTICLE

Ti(IV) nanocluster as a promoter on semiconductor photocatalysts for oxidation of organic compounds

Ryota Inde,^{a,c} Min Liu,^{b,c} Daiki Atarashi,^a Etsuo Sakai,^a Masahiro Miyachi^{a,*}

Received 00th January 20xx,
Accepted 00th January 20xx

DOI: 10.1039/x0xx00000x

www.rsc.org/

The surface modification of semiconductors is a potential approach for the development of visible-light-sensitive photocatalysts. Here, we report that amorphous Ti(IV) nanoclusters grafted onto metal oxide photocatalysts function as efficient promoters for the oxidation of organic contaminants, including acetaldehyde or 2-propanol. Ti(IV) nanoclusters were facilely grafted onto metal oxides like titanium dioxide (TiO₂) and tungsten trioxide (WO₃) by using a simple impregnation method. The photocatalytic activity of Ti(IV) nanocluster-grafted TiO₂ under UV-light irradiation was much higher than that of bare TiO₂, even though the surface area and photon absorption of these two materials were identical. The improved photocatalytic activity was attributable to hole trapping by the Ti(IV) nanoclusters, which form a unique electronic structure, resulting in efficient charge separation. Kelvin probe force microscopy analysis revealed that the highest occupied molecular orbital (HOMO) of the Ti(IV) nanoclusters has a more negative potential than the valence band of bulk rutile TiO₂, which allows hole transfer from bulk TiO₂ to the Ti(IV) nanoclusters. The grafting of Ti(IV) nanoclusters was also shown to increase the photocatalytic activity of WO₃. WO₃ also requires reduction reaction promoters, such as Cu(II) nanoclusters, because of the low energy of its conduction band (CB). The grafting of both Ti(IV) and Cu(II) nanoclusters onto WO₃ resulted in the highest reaction rate reported to date for the decomposition of gaseous 2-propanol under visible-light irradiation.

1. Introduction

Photocatalytic reaction rates depend on two main parameters: absorbed photon number of the semiconductor photocatalyst and quantum efficiency of the chemical reaction mediated by excited charge carriers. Titanium dioxide (TiO₂) is one of the most well-known photocatalysts;^{1–5} however, due to its large bandgap, TiO₂ only exhibits limited photon absorption under irradiation from sunlight or indoor lighting apparatus. Further, photoexcited electrons and holes in TiO₂ are easily recombined at surface sites or in bulk through radiative process. To improve the photocatalytic activity, the two main approaches are to increase photon absorption and improve charge separation efficiency. However, these two approaches contradict each other, because if attempts are made to increase absorbed photon number by doping with cations or anions to extend the responsive wavelength of the material toward visible light,^{6–11} the quantum efficiency of the resulting material would deteriorate, as the doping sites act as recombination centers. For example, nitrogen-doped TiO₂ is capable of absorbing visible light,^{12–16} but the quantum

efficiency of this material under visible light is several orders of magnitude lower than that of pure TiO₂ under UV light.^{14, 16} Photoexcited holes in nitrogen levels are localized and have limited mobility and less oxidation power as compared to those in the valence band of oxygen 2p orbitals.¹⁴ For these reasons, it is difficult to develop efficient visible-light sensitive photocatalysts by the doping of semiconductors.

In addition to doping, the surface modification of metal oxide photocatalysts is another potential strategy to improve photocatalytic activity. For example, noble metal cocatalyst promoters, such as Pt, Au, Ag, Pd, and Rh, were grafted onto TiO₂ surface to improve charge separation efficiencies.^{17–24} But these cocatalysts only promoted UV light activities of TiO₂ and were composed of expensive rare metals. Recently, the efficient visible light sensitive photocatalysts with high quantum yield have been developed on the basis of economical Cu(II) or Fe(III) nanoclusters grafted TiO₂.^{25–30} These materials utilize visible light for photocatalysis through an interfacial excitation process,³¹ with the Cu(II) and Fe(III) clusters additionally serving as efficient reduction reaction promoters for oxygen reduction. As a result of the structural optimization of Cu(II) or Fe(III) by our group, the quantum efficiencies of Cu(II) or Fe(III)-grafted TiO₂ were improved to 68.7%³² and 53.5%,³³ respectively. While Cu(II) and Fe(III) clusters accelerate reduction reaction, we also reported that Ti(IV) clusters promote the oxidation of organic contaminants, and it was demonstrated that Cu(II) and Ti(IV)-grafted TiO₂ has the highest quantum yield for the decomposition of alcohol.³⁴

^a Graduate School of Science and Engineering, Tokyo Institute of Technology

^b Research Center of Advanced Science and Technology, The University of Tokyo

^c R. Inde and M. Liu contributed equally to this work.

* to whom corresponding should be addressed.

E-mail: mmiyauchi@ceram.titech.ac.jp

Electronic Supplementary Information (ESI) available.

See DOI: 10.1039/x0xx00000x

Ti(IV) clusters are composed of amorphous titanium oxide with the size of several nanometers scale.

Herein, we comprehensively studied the function of Ti(IV) nanoclusters as general cocatalysts for the oxidation of organic contaminants. In addition to the TiO₂ photocatalytic system, Ti(IV) nanoclusters were grafted onto WO₃ particles, and the photocatalytic oxidation reactions of the resulting material for acetaldehyde, 2-propanol, and water oxidation were investigated. Promoting effect of Ti(IV) nanoclusters on TiO₂ photocatalyst was investigated under UV light irradiation, while that on WO₃ was measured under blue light irradiation, respectively. Further, Kelvin probe force microscopy (KPFM) was used to examine the electronic structure of Ti(IV) nanocluster-grafted TiO₂ and the mechanism of charge transport between nanoclusters and bulk. Following optimization of the grafting process, Cu(II) and Ti(IV) nanocluster-grafted WO₃ exhibited the highest reaction rate under visible-light irradiation reported to date among visible-light-sensitive photocatalysts.

2. Experimental

2.1 Preparation of Ti(IV) nanocluster-grafted TiO₂ (Ti(IV)-TiO₂)

Commercial rutile TiO₂ powder (MT-150A, Tayca Co.) was used as starting material. To prepare the material for grafting, the TiO₂ powder was heated at 950 °C for 3 h in air to improve the crystallinity. The powder was then placed in 6 mol/L HCl aqueous at 90 °C for 3 h under stirring to remove surface ionic contamination.³² After washing with distilled water, the TiO₂ powder was collected by filtration and dried at 80 °C for 24 h.

The grafting of Ti(IV) nanoclusters onto TiO₂ was performed using a simple impregnation method. First, titanium tetrachloride (TiCl₄; Wako Pure Chemical Industries, Ltd.) was added to a 0.5 mol/L aqueous solution of hydrochloric acid (HCl) on ice bath until the TiCl₄ concentration reached 0.5 mol/L. For the grafting of Ti(IV) nanoclusters onto TiO₂, the prepared Ti⁴⁺ solution was added to the TiO₂ suspension until reaching a concentration of 0.25 wt% versus TiO₂, and the resulting suspension was heated at 90 °C for 1 h under stirring. After cooling the solution to room temperature, the precipitated powder was washed with distilled water and filtered. The washing and filtering process was repeated three times. The synthesized Ti(IV) nanocluster-grafted TiO₂ (Ti(IV)-TiO₂) was dried at 80 °C for 24 h. For KPFM analysis, Ti(IV) nanoclusters were grafted onto the surface of single crystals of rutile (110) TiO₂ using the same procedure.

2.2 Preparation of Cu(II) and Ti(IV) nanocluster-grafted WO₃ (Cu(II)-Ti(IV)-WO₃)

As the conduction band of WO₃ is lower than that of TiO₂, WO₃ requires a reduction reaction promoter to drive the multi-electron reduction of oxygen.²⁵ Thus, in addition to Ti(IV) clusters, Cu(II) nanoclusters were also grafted onto crystalline WO₃ powder (Showa Denko Ceramics Co.). Ti(IV) clusters were firstly grafted onto WO₃ powder using the above-described method for TiO₂. Cu(II) nanoclusters were then grafted onto

Ti(IV) nanocluster-grafted WO₃ by adding an aqueous solution of copper chloride (CuCl₂), which was used as a source of Cu²⁺ ions, to the Ti(IV)-WO₃ suspension at a final Cu²⁺ concentration of 0.1 wt% versus Ti(IV)-WO₃. The resulting solution was heated to 90 °C for 1 h under stirring. After cooling the solution to room temperature, the precipitated Cu(II) and Ti(IV) nanocluster-grafted WO₃ (Cu(II)-Ti(IV)-WO₃) was repeatedly washed with distilled water and filtered (three times). The obtained Cu(II)-Ti(IV)-WO₃ powder was dried at 80 °C for 24 h.

2.3 Characterization

Crystal structures of the obtained powder samples were determined by X-ray diffraction (XRD; Rigaku, SmartLab) using Cu- α X-rays ($\lambda=1.5418$ Å). UV-visible (UV-vis) absorption spectra were recorded using a diffuse reflection method with a spectrophotometer equipped with an integration sphere unit (V-670; Jasco). The specific surface areas of the powder samples were measured by the Brunauer-Emmet-Teller (BET) technique³⁵ using nitrogen gas and surface area analyzer (Micromeritics Gemini V, Shimadzu). Sample morphologies were observed by scanning electron microscopy (SEM; VE-9800SP, Keyence) and transmission electron microscopy (TEM; JEM-2010F, JOEL). Photoluminescence (PL) spectra were obtained using a Hitachi F-4500 fluorophotometer at an excitation wavelength of $\lambda=325$ nm at room temperature. The surface topographic and potential images of single-crystal rutile TiO₂ substrates were observed by atomic force microscopy (AFM) and KPFM (SPM-9700, Shimadzu). AFM and KPFM measurements were performed in the tapping mode using platinum and iridium-coated cantilevers (Point Probe EFM, tip curvature: 20 nm; Nano World, Ltd.) under ambient conditions.³⁶ Surface compositions were studied by X-ray photoelectron spectroscopy (XPS; model 5600, Perkin-Elmer). Binding energy data were calibrated with reference to the C 1s signal at 284.5 eV. Electrochemical measurements were performed with an electrochemical workstation (PGSTAT302N, Metrohm Autolab, Inc.) in a 0.2 M aqueous solution of Na₂SO₄. An Ag/AgCl (3M) electrode and a platinum plate were used as the reference and counter electrodes, respectively. For the fabrication of electrochemical electrodes, 4 mg of catalyst powder was dispersed in 1 mL of a 4:1 mixture of water:ethanol and 80 μ L Nafion solution, and the resulting mixture was sonicated for 30 min. 5 μ L of the sonicated solution was drop-casted onto the surface of a glassy carbon disk electrode at a catalyst loading of 0.285 mg/cm².

2.4 Photocatalytic activity measurements

Photocatalytic activities were measured by the generation rate of CO₂ during the oxidation of acetaldehyde (CH₃CHO + 5/2O₂ \rightarrow 2CO₂ + 2H₂O).³⁷ For the measurements, 0.1 g powder samples were dispersed on a glass dish (area: 7.07 cm²), which was then placed in a closed glass container (500-mL capacity). The gas in the container was displaced with synthetic humid air (N₂: 80%, O₂: 20%, humidity: 10%, temperature: 293 K). Before performing the photocatalytic measurements, the samples were irradiated with light for more than 24 h as a

pretreatment step to remove organic contaminants. The irradiated light used for pretreatment was the same as was used for photocatalysis testing: UV light (310-410 nm) emitted from a 10 W black light bulb (Toshiba) for the TiO₂ samples, and blue LED (420-530 nm) for the WO₃ samples. After the pre-irradiation treatment, the atmosphere of the glass container was replaced with fresh synthetic humid air (N₂: 80%, O₂: 20%, humidity: 10%, temperature: 293 K), and concentrated acetaldehyde gas (5% CH₃CHO in N₂ balance; Taiyo Toyo Sanso Co.) was then injected into the system. The initial quantity of acetaldehyde was approximately 4 μmol for TiO₂ samples and 6 μmol for WO₃ samples. The samples were kept in the dark until the adsorption reached equilibrium and were then irradiated with light. The spectra of the UV and LED light sources used for the irradiation of TiO₂ irradiation was black light (310-410 nm), while that for WO₃ was blue LED (420-530 nm), and those spectra were shown in the absorption spectra (Fig. 4a and b). CO₂ and acetaldehyde concentrations under light irradiation were measured by micro gas chromatography (3000 Micro GC, Inficon). Photocatalytic decomposition of gaseous 2-propanol (CH₃CHOHCH₃ + 9/2O₂ → 3CO₂ + 4H₂O) was also measured in a similar manner to that used for acetaldehyde. The oxidation of 2-propanol generates gaseous acetone and CO₂ as reaction products, and these gasses were detected using a gas chromatograph (GC-8A, Shimadzu) equipped with a flame ionization detector (FID) and methanizer. Water oxidation properties were evaluated on Ti(IV)-TiO₂ and bare TiO₂ powder under UV-light irradiation in aqueous solution containing sacrificial AgNO₃ agent (50 mmol/L). After purging the aqueous solution and headspace with argon gas, the cell was illuminated with light emitted from a 150-W Hg-Xe lamp. Evolved O₂ gas was detected using an on-line gas chromatograph (GC-8A, Shimadzu Co.) equipped with a molecular sieve-packed column and using Ar as the carrier gas.

3. Results

3.1. Structural, optical, and electronic properties of Ti(IV)-TiO₂ and Ti(IV)-WO₃ photocatalysts

To investigate the morphology of surface-grafted Ti(IV) nanoclusters, the synthesized Ti(IV)-TiO₂ and Ti(IV)-WO₃ photocatalysts were observed by TEM (Fig. 1). Examination of the TEM images revealed that amorphous nanoclusters of approximately 5 nm in size were deposited on the crystalline particles of TiO₂ or WO₃. The results of energy dispersive X-ray (EDX) spectroscopy analyses are presented in panels (c) and (d), which correspond to points (i) and (ii) in the TEM image shown in panel (b). An EDX signal for titanium was clearly observed at point (i), but was not detected at point (ii), indicating that the small particles observed in the TEM images corresponded to Ti(IV) nanoclusters. The EDX signal corresponding to molybdenum (Mo) was attributable to a contaminant from the sample grid holder. Further, high resolution (HR)-TEM images on the different position from Fig. 1 were recorded (Fig. S1 in the supporting information), and the Ti(IV) clusters were

clearly observed with nanometer scale size. In addition to HR-TEM images, low magnification TEM images with large scale are shown in the supporting information (Fig. S2), and we could confirm that the Ti(IV) nanoclusters were highly dispersed over the surface of TiO₂ and WO₃.

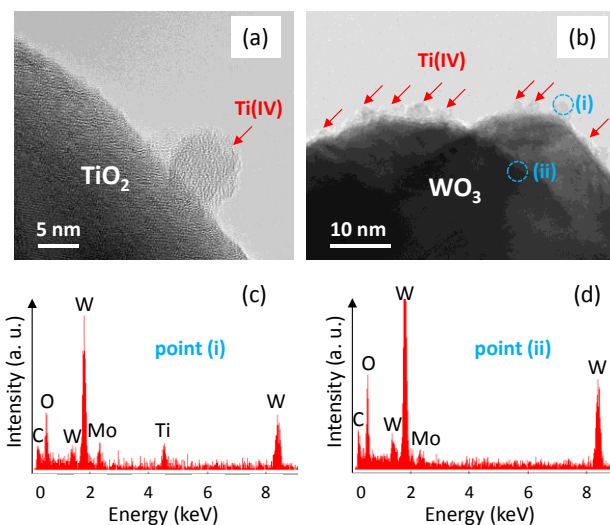


Fig. 1 TEM images for Ti(IV)-TiO₂ (a), and Ti(IV)-WO₃ (b). Panels (c) and (d) are point EDX spectra of the Ti(IV)-WO₃ on point (i) and point (ii), which are indicated in panel (b).

The surface compositions and elemental chemical states of the photocatalytic samples were investigated by XPS (Fig. 2 and Fig. S3, Supporting Information). The Ti 2p core-level spectra indicated that Ti(IV) nanoclusters were successfully grafted onto WO₃, as indicated by the well-resolved Ti 2p_{1/2} and Ti 2p_{3/2} spectral lines at 464.0 and 458.3 eV, respectively (Fig. 2a and Fig. S3, Supporting Information), those are in agreement with those previously reported for Ti⁴⁺.⁷⁻⁹ No shoulder peaks associated with Ti³⁺ or Ti²⁺ were observed at the lower energy side of the spectra. In the W 4f core-level spectra (Fig. 2b), no obvious differences were seen in the chemical states of elemental W,³⁸ demonstrating that the surface grafting of Ti(IV) nanoclusters did not affect the bonding structure of the tungsten ions.

The XRD patterns of nanocluster-grafted TiO₂ and WO₃ are shown in Fig. 3, and those of bare TiO₂ and WO₃ powders are also shown for comparison. All diffraction peaks of the TiO₂ samples were assigned to rutile phase, and those of WO₃ samples originated from the sole monoclinic WO₃ phase. The XRD patterns of nanocluster-grafted TiO₂ and WO₃ were identical to those of bare TiO₂ and WO₃, indicating that the grafting of the Ti(IV) nanoclusters did not result in additional crystal formation. Additional analysis by SEM did not reveal any obvious differences between the nanocluster-grafted samples and bare samples under the maximum resolution condition of the SEM apparatus (Fig. S4, Supporting Information). Based on the XRD, XPS and SEM results, it was concluded that the Ti(IV) nanoclusters were highly dispersed on the surfaces of TiO₂ or WO₃ as amorphous phase, and did not affect the crystal structure or morphologies of raw TiO₂ and WO₃ particles.

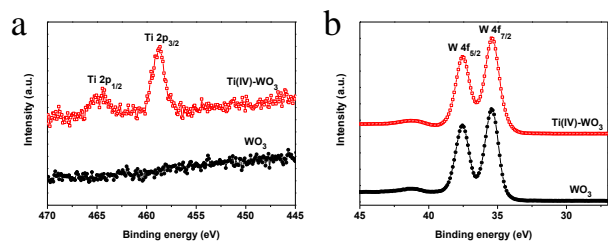


Fig. 2 Ti 2p (a) and W 4f (b) core-level spectra of WO_3 and Ti(IV)-WO_3 respectively.

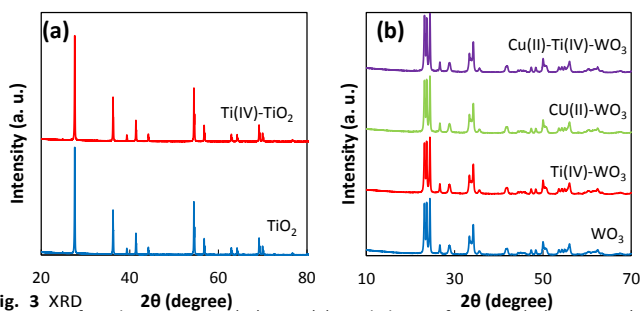


Fig. 3 XRD patterns of rutile TiO_2 and Ti(IV)-TiO_2 (a), and those of WO_3 , Ti(IV)-WO_3 , Cu(II)-WO_3 and $\text{Cu(II)-Ti(IV)-WO}_3$ (b), respectively.

The BET surface areas for the nanocluster-grafted TiO_2 and WO_3 samples are listed in Table 1. No marked changes in specific surface area were detected upon the grafting of Ti(IV) nanoclusters onto TiO_2 , whereas a slight increase in BET surface area was observed for WO_3 . We also confirmed the existence of Cu(II) species on the $\text{Cu(II)-Ti(IV)-WO}_3$ sample by XPS (Fig. S5, Supporting Information).

Fig. 4 shows UV-vis absorption spectra of the TiO_2 (a) and WO_3 samples (b). Strong absorption was observed below 410 nm for TiO_2 , whereas the WO_3 samples absorbed light below 480 nm. These results are consistent with the bandgap of TiO_2 (3.0 eV) and WO_3 (2.6 eV). Notably, no differences were detected between the nanocluster-grafted and bare TiO_2 and WO_3 samples, indicating that the Ti(IV) nanoclusters did not affect the light absorption properties of TiO_2 or WO_3 . Fig. 4 also shows the spectra of light sources used in the photocatalytic testing. The light spectra of the black light bulb and blue LED, which were used for the irradiation of the TiO_2 and WO_3 samples, respectively, overlapped with the optical absorption of photocatalysts, implying that both semiconductors were excited by the light sources used in the present experiment.

To examine the electronic structure of the Ti(IV) nanoclusters, single crystals of rutile TiO_2 grafted with Ti(IV) nanoclusters were analyzed by KPFM, which is a powerful tool to determine the work function or Fermi level of semiconductors at nanometer-sized scale resolution. KPFM images are therefore very informative for assessing the possibility of charge transport between nanoclusters and bulk semiconductor.³⁶ We used atomically flat single crystals of rutile TiO_2 with an exposed (110) plane surface, which is one of the most thermodynamically stable crystal planes.³⁹⁻⁴⁰ Fig. 5 shows AFM and KPFM images for bare rutile TiO_2 and single crystals of Ti(IV) nanocluster-grafted rutile TiO_2 . AFM imaging

Table 1 BET surface area for powder samples (unit: m^2/g)

TiO_2	Ti(IV)-TiO_2	WO_3	Cu(II)-WO_3	Ti(IV)-WO_3	$\text{Cu(II)-Ti(IV)-WO}_3$
5.36	5.23	8.81	9.36	9.29	10.02

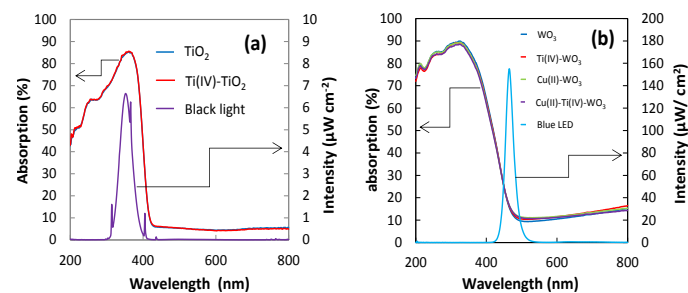


Fig. 4 UV-vis absorption spectra of bare TiO_2 , Ti(IV)-TiO_2 and spectrum of black light used in evaluation of the photocatalytic activities (a). UV-vis absorption spectra of WO_3 , Ti(IV)-WO_3 , Cu(II)-WO_3 , $\text{Cu(II)-Ti(IV)-WO}_3$ and spectrum of blue LED used in evaluation of the photocatalytic activities (b).

revealed that the surface of rutile single crystal was very smooth, whereas that of the Ti(IV) nanocluster-grafted sample was covered with nanometer-scale sized structures, indicating that the Ti(IV) nanoclusters were successfully grafted onto the bulk rutile TiO_2 . The KPFM images also show maps of the work function for the same area shown in the AFM images, and it was noted that the work function of the Ti(IV) nanoclusters was smaller than that of bulk rutile TiO_2 . The KPFM results imply that Ti(IV) nanoclusters and bulk rutile TiO_2 have different work functions, as discussed in more detail later. In addition, electrochemical Mott-Schottky analyses showed that the flat band potential of Ti(IV)-WO_3 was more negative than that of WO_3 (Fig. S6, Supporting Information), suggesting that the LUMO level of the Ti(IV) clusters was more negative than the conduction band minimum of WO_3 . The presence of polar structures at the interface cause charge transport in heterogeneous semiconductors.⁴¹⁻⁴³

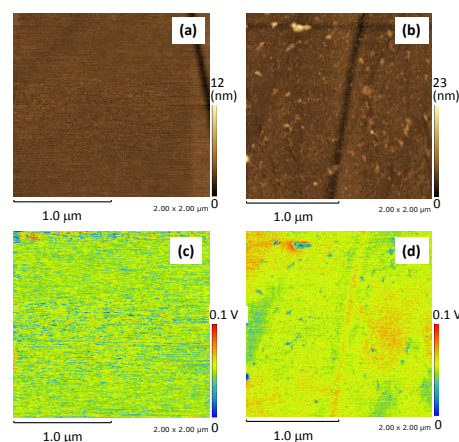


Fig. 5 Topographic AFM images for bare rutile TiO_2 single crystal (a) and Ti(IV)-TiO_2 (b). KPFM images of bare TiO_2 (c) and Ti(IV)-TiO_2 (d), respectively. The surface crystal face of rutile TiO_2 was (110) plane for all samples.

3.2 Photocatalytic activities

Fig. 6 shows the photocatalytic activities of the bare and Ti(IV)-grafted TiO_2 and WO_3 samples for acetaldehyde oxidation. The oxidation of acetaldehyde was monitored by measuring the concentrations of the generated CO_2 under light irradiation. The CO_2 generation rate of TiO_2 under UV-light irradiation was greatly increased by the grafting of Ti(IV) nanoclusters (Fig. 6a). We also monitored changes in the acetaldehyde concentration under dark conditions and observed similar trends for both the bare and Ti(IV)-grafted TiO_2 samples indicating that bare TiO_2 and Ti(IV)- TiO_2 adsorbed similar amounts of acetaldehyde, a finding that is consistent with the fact that two materials have identical BET surface areas. A previous study also reported that Ti(IV) nanocluster-grafted TiO_2 and bare TiO_2 powder have similar zeta potentials.³⁴ Further, these two materials also exhibited identical optical absorption profiles (Fig. 4a). Even though the photon absorption and surface adsorption properties of Ti(IV)- TiO_2 were the same as those of bare TiO_2 , Ti(IV)- TiO_2 has a markedly higher reaction rate than that of bare TiO_2 . Taken together, these results indicate that the quantum efficiency for charge separation was improved by the surface grafting of Ti(IV) nanoclusters, as the present photocatalytic testing was conducted under light-limited conditions.³⁷

The photocatalytic oxidation of acetaldehyde by WO_3 samples under blue LED irradiation was also measured (Fig. 6b). As the initial concentration of acetaldehyde was approximately 6 μmol , the CO_2 concentration would reach 12 μmol upon the complete oxidation of acetaldehyde, as acetaldehyde contains two carbon atoms. In the case of bare WO_3 , the CO_2 concentration was saturated at approximately 5 μmol , indicating that the acetaldehyde was not completely oxidized. This phenomenon has been previously observed for bare WO_3 samples, as the CB of WO_3 is not sufficiently high to reduce oxygen molecules, resulting in the electron accumulation and reduction of WO_3 itself.⁴⁴ Thus, bare WO_3 cannot completely decompose acetaldehyde without cocatalyst promoters, and acetaldehyde is only partially oxidized to intermediate products, such as acetic acid. However, upon the grafting of Ti(IV) nanoclusters onto WO_3 , the reaction rate increased in the early stages of irradiation, although CO_2 generation was also saturated at 6 μmol . In contrast to bare and Ti(IV)-grafted

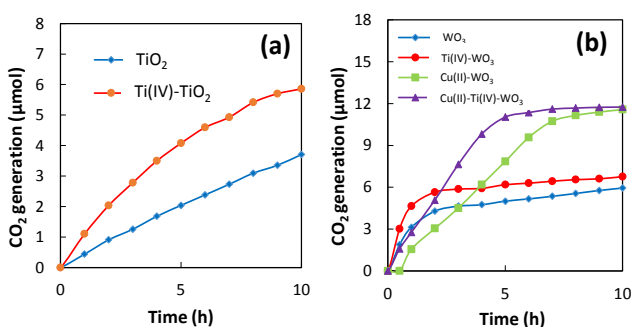


Fig. 6 Photocatalytic activities for oxidation of gaseous acetaldehyde. (a): TiO_2 samples under UV light (b): WO_3 samples under visible light. A 10 W cylindrical black light bulb was used for UV irradiation onto TiO_2 , while a blue LED was used for visible light irradiation onto WO_3 .

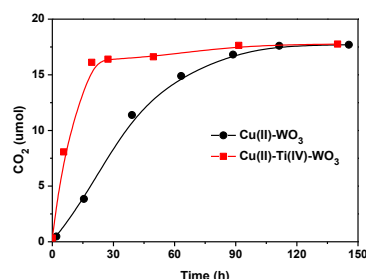


Fig. 7 Photocatalytic activities for oxidation of 2-propanol for WO_3 samples under a blue LED irradiation.

WO_3 , Cu(II)-grafted WO_3 completely decomposed acetaldehyde into CO_2 , which reached a final concentration of 12 μmol . Although the surface area of the nanocluster-grafted samples was slightly higher than that of bare WO_3 , the observed difference in the decomposition efficiency cannot be simply explained by differences in the surface area or adsorption of target molecules. Cu(II) nanoclusters are known to drive the multi-electron reduction of oxygen to hydrogen peroxide.⁴⁵ Notably, after further grafting Ti(IV)- WO_3 with Cu(II) nanoclusters, the resulting Cu(II)-Ti(IV)- WO_3 sample exhibited excellent photocatalytic oxidation activity under blue light irradiation, as was observed by the complete decomposition of acetaldehyde into CO_2 . The optical absorption and adsorbability of the Ti(IV)- WO_3 and Cu(II)-Ti(IV)- WO_3 samples were similar, indicating that the Ti(IV) grafting improves the quantum efficiency (QE) of WO_3 , as well as TiO_2 , photocatalysts.

The oxidation of gaseous phase 2-propanol by the TiO_2 and WO_3 samples were also evaluated (Fig. 7 and Fig. S7, Supporting Information). The Ti(IV)- TiO_2 and Cu(II)-Ti(IV)- WO_3 samples exhibited strong photocatalytic activity for 2-propanol decomposition under blue light irradiation. The calculated QE of the Cu(II)-Ti(IV)- WO_3 sample increased to 21.2% and was nearly two-fold higher than that reported for Cu(II)- WO_3 ²⁵ (Table S1, Supporting Information). The reaction rate of Cu(II)-Ti(IV)- WO_3 reached 0.83 $\mu\text{mol}/\text{h}$ at an absorbed photon number of 3.91×10^{15} quanta/ cm^2/sec , which is the highest rate reported to date among visible-light-sensitive photocatalysts under blue light irradiation. The reaction rates per catalysis mass were estimated to be 2.77 and 1.56 $\mu\text{mol}/\text{h}/\text{g}$ for Cu(II)-Ti(IV)- WO_3 and Cu(II)- WO_3 , respectively. We also evaluated the photocatalytic activities under a commercial white light emitting diode (LED) to prove our photocatalyst is promising for practical indoor application. Photocatalytic oxidation activities under white LED were shown in the supporting information (Fig. S8), and the Cu(II)-Ti(IV)- WO_3 exhibited excellent visible light activity even under a commercial white LED.

Further, the stability of photocatalyst is very important for the practical applications. In particular, WO_3 causes photochromic reaction by the accumulation of photogenerated electrons in itself, which deteriorates its photocatalytic activity.⁴⁴ Thus, we have conducted the photocatalysis cycling test on Cu(II)-Ti(IV)- WO_3 for 5 times for

oxidation of 2-propanol under blue light irradiation, and the results are shown in Fig. 8. Initial concentration of 2-propanol was set at $6.0 \pm 0.3 \mu\text{mol}$, thus the CO_2 must be reached at 17.1–18.9 μmol after complete oxidation of 2-propanol. We have confirmed that the photocatalytic reaction rate of the Cu(II)-Ti(IV)- WO_3 has been maintained and it can completely oxidizes 2-propanol to CO_2 over 5 times cycling test, indicating its high stability under photon irradiation condition.

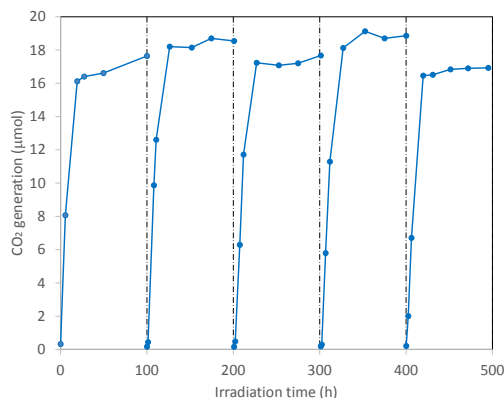


Fig. 8 Cycling measurements of the 2-propanol oxidation over Ti(IV)-Cu(II)- WO_3 under blue light irradiation.

In addition to the photocatalytic oxidation of organic compounds, the effect of Ti(IV) grafting on water oxidation (O_2 generation) as a half reaction of water splitting was also investigated (Fig. S9, Supporting Information,). However, Ti(IV) grafting did not enhance water oxidation, indicating that Ti(IV) nanoclusters selectively promote the oxidation of organic molecules in gaseous phase, but do not promote four-electron oxidation reactions in water medium.

4. Discussion

The present experimental results revealed that the grafting of Ti(IV) nanoclusters onto TiO_2 and WO_3 semiconductors improves their photocatalytic activities, however, this effect is not simply attributable to changes in the optical absorption or surface adsorption properties of the photocatalyst, but is largely influenced by efficient charge separation. KPFM imaging of single crystalline TiO_2 revealed that the work function of Ti(IV) nanoclusters is smaller than that of bulk rutile TiO_2 , implying that the Fermi level of Ti(IV) nanoclusters is more negative than that of bulk rutile TiO_2 . Thus, the photogenerated holes in the valence band of TiO_2 can be transferred to the surface-grafted Ti(IV) nanoclusters. Although we were not able to analyze single crystals of WO_3 , Mott-Schottky plots showed that the flat band potential of Ti(IV)- WO_3 was more negative than that of WO_3 . (Fig. S6, supporting information). Because WO_3 is an n-type semiconductor, its flat band potential is located just below its conduction band minimum (CBM). The results of the present Mott-Schottky analysis implies that the LUMO of Ti(IV) clusters is more negative than the CBM of WO_3 . These results are consistent with the KPFM analysis of TiO_2 . Further, the measured photoluminescence (PL) spectra of the TiO_2 and

WO_3 samples confirmed that the grafting of Ti(IV) nanoclusters reduced the recombination of electron hole pairs, resulting in better charge separation efficiency (Fig. S10, Supporting Information). As WO_3 has a deeper VB compared to TiO_2 ,⁴⁶⁻⁴⁷ hole transfer would be feasible from the VB of WO_3 to Ti(IV) nanoclusters. Nolan et al. simulated the electric structure of nanometer-scale TiO_2 clusters by first principle calculations and compared the LUMO and HOMO levels of these nanoclusters with those of bulk rutile TiO_2 . The results of these calculations revealed that both the LUMO and HOMO levels of nanosized TiO_2 clusters were more negative than the CB and VB of bulk rutile TiO_2 , whereas the bandgap of nanosized TiO_2 was 0.1 eV wider than bulk TiO_2 , owing to the quantum confinement effect.⁴⁸ The calculated HOMO levels of Ti_2O_4 , Ti_3O_6 , and Ti_4O_8 molecules were 0.2, 1.3, and 0.9 eV more negative than the VB of rutile TiO_2 . Based on the findings from these reports and the present experimental results, the predicted electronic structures for Ti(IV)- TiO_2 and Cu(II)-Ti(IV)- WO_3 are schematically shown in Fig. 9. The HOMO level of the Ti(IV) nanoclusters would be more negative than the VB potential of bulk TiO_2 and WO_3 . On the other hand, the redox potential of Cu(II) nanoclusters is reported to be +0.16 V (vs. NHE at pH=0).^{25, 28}

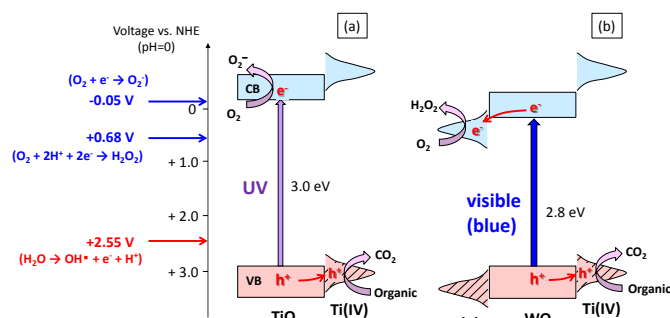
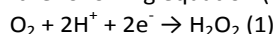


Fig. 9 Assumed electronic structures for Ti(IV)- TiO_2 (a) and Cu(II)-Ti(IV)- WO_3 (b), respectively.

Next, we discuss the excited states of nanoclusters. Upon the UV-light irradiation of Ti(IV)- TiO_2 , electrons in the VB are excited to the CB of TiO_2 and have sufficient potential to cause the single-electron reduction of oxygen molecules to superoxide anion radicals (O_2^-). Photogenerated holes in the VB of TiO_2 can be injected into the grafted Ti(IV) nanoclusters, because the HOMO level of the nanoclusters is more negative than the VB of TiO_2 . Electron spin resonance (ESR) spectra of Ti(IV)- TiO_2 and bare TiO_2 under light irradiation were previously measured, and two types of photogenerated holes formed peaks at $g = 2.004$ and 2.007 for Ti(IV)- TiO_2 , whereas only the $g = 2.004$ peak was observed in bare TiO_2 .³⁴ In Ti(IV) nanocluster-grafted TiO_2 , a portion of excited holes might become trapped at different sites from those in bare TiO_2 , because the ESR peak positions are dependent on the coordination environment. The $g = 2.004$ ESR peak is assigned to photoexcited holes in the VB of bulk TiO_2 as O^- species, whereas the $g = 2.007$ peak is attributable to photoexcited holes in Ti(IV) clusters. Similar hole trapping is expected to occur in the WO_3 system, as the VB of WO_3 is sufficiently deep

to enable hole transfer to Ti(IV) nanoclusters.⁴⁹ The grafting of Ti(IV) nanoclusters as promoter cocatalysts was potentially applicable for other semiconductors such as zinc oxide (ZnO) and nitrogen doped TiO₂, and their visible light activities under blue light were shown in the supporting information (Fig. S11 and S12), revealing the Ti(IV) grafting is also very effective to the enhancement of photocatalytic activities of ZnO and doped TiO₂ other than pristine TiO₂ or WO₃. On the basis of these results, efficient charge separation is expected by hole trapping in Ti(IV) nanoclusters. In particular for the WO₃ photocatalyst, it is also important to consider the promotion of reduction reactions, because its CB is not sufficiently high to drive the single-electron reduction of oxygen molecules.^{44, 50-52} Recently, Cu(II) nanoclusters were reported to drive the multi-electron reduction of oxygen to produce hydrogen peroxide (H₂O₂), as shown in the following equation (1):



The redox potential of this multi-electron reaction is +0.68 V (vs NHE at pH=0), which is more positive than that of Cu(II)/Cu(I) nanoclusters (+0.16 V). Previous X-ray absorption and ESR analyses on the excited states of Cu(II) nanoclusters revealed that Cu(I) species are formed under light irradiation in the absence of oxygen, whereas Cu(II) species are stable in the presence of oxygen.^{26, 45} These results strongly suggest that the excited electrons in Cu(II) nanoclusters strongly interact with oxygen molecules in air. In addition, Nosaka et al.⁴⁵ experimentally detected the formation of H₂O₂ from Cu(II)-WO₃ under visible-light irradiation.

Based on the present experimental data and electronic structure analysis, we can conclude that Ti(IV) nanoclusters act as oxidation reaction promoters, whereas Cu(II) nanoclusters act as reduction reaction promoters. Both Cu(II) and Ti(IV) nanocluster-grafted WO₃ exhibited the highest reaction rates among previously reported photocatalysts for 2-propanol oxidation under blue LED irradiation (0.83 μmol/h with photon absorption at 3.91 × 10¹⁵ quanta/cm²/sec) with long term stability. Notably, however, Ti(IV) nanoclusters are not universal cocatalysts for oxidation reaction, particularly for four-electron oxidation reactions, such as water oxidation. Our experimental results demonstrate that Ti(IV) nanoclusters effectively promote the oxidation of organic contaminants, including aldehydes and alcohols, and would therefore be useful for the modification of photocatalysts designed for environmental remediation, such as air purification and disinfection.

5. Conclusions

We have succeeded in developing a Ti(IV) nanocluster-based promoter cocatalyst for the oxidation of organic compounds. KPFM analysis indicated that Ti(IV) nanoclusters have a specific electronic potential structure that is preferential for hole trapping. The grafting of Ti(IV) nanoclusters increases the UV-light activity of TiO₂ and also enhances the visible-light activity of Cu(II)-grafted WO₃. Both Cu(II) and Ti(IV) nanocluster-grafted WO₃ exhibited the highest reaction rate for the oxidation of gaseous 2-propanol under blue light irradiation

among previously reported photocatalysts. Ti(IV) nanoclusters are composed of non-toxic elements and can be grafted onto various semiconductors using a simple wet impregnation method, which greatly reduces the cost of mass-fabrication processes. The grafting of nanoclusters as promoter cocatalysts is potentially applicable for other semiconductors with deep valence bands, such as ZnO, SrTiO₃, BiVO₄, and SnO₂, and represents a strategic approach for the development of efficient photocatalysts for environmental remediation.

Author Contributions

R. Inde and M. Liu designed and conducted the experiments, synthesized the materials, and wrote the manuscript. R. Inde and M. Liu contributed equally to this work. D. Atarashi and E. Sakai provided important suggestions. M. Miyauchi conceived this project and wrote the manuscript.

Acknowledgements

This research was supported by NEDO and JST. We would like to thank Prof. Y. Nosaka and Dr. M. Nishikawa at Nagaoka University of Technology for their discussion of ESR analysis, and we gratefully acknowledge Dr. Y. Kuroda at Showa Denko Ceramics Co. for providing WO₃ powder. We also thank Mr. A. Genseki at the Center for Advanced Materials Analysis of the Tokyo Institute of Technology for helping with the TEM analysis. We also acknowledge Mr. Greg Newton for the critical reading of the manuscript.

Notes and references

- 1 A. Fujishima and K. Honda, *Nature*, 1972, **238**, 37-38.
- 2 K. Hashimoto, H. Irie and A. Fujishima, *Japanese Journal of Applied Physics*, 2005, **44**, 8269.
- 3 A. L. Linsebigler, G. Lu and J. T. Yates, *Chemical Reviews*, 1995, **95**, 735-758.
- 4 M. R. Hoffmann, S. T. Martin, W. Choi and D. W. Bahnemann, *Chemical Reviews*, 1995, **95**, 69-96.
- 5 B. Ohtani, Y. Ogawa and S.-i. Nishimoto, *The Journal of Physical Chemistry B*, 1997, **101**, 3746-3752.
- 6 W. Choi, A. Termin and M. R. Hoffmann, *The Journal of Physical Chemistry*, 1994, **98**, 13669-13679.
- 7 H. Kato and A. Kudo, *The Journal of Physical Chemistry B*, 2002, **106**, 5029-5034.
- 8 A. Kudo, R. Niishiro, A. Iwase and H. Kato, *Chemical Physics*, 2007, **339**, 104-110.
- 9 N. Serpone, *The Journal of Physical Chemistry B*, 2006, **110**, 24287-24293.
- 10 M. Miyauchi, M. Takashio and H. Tobimatsu, *Langmuir : the ACS journal of surfaces and colloids*, 2004, **20**, 232-236.
- 11 T. Ohno, T. Mitsui and M. Matsumura, *Chemistry Letters*, 2003, **32**, 364-365.
- 12 R. Asahi, T. Morikawa, T. Ohwaki, K. Aoki and Y. Taga, *Science*, 2001, **293**, 269-271.
- 13 M. Mrowetz, W. Balcerski, A. J. Colussi and M. R. Hoffmann, *The Journal of Physical Chemistry B*, 2004, **108**, 17269-17273.
- 14 H. Irie, Y. Watanabe and K. Hashimoto, *The Journal of Physical Chemistry B*, 2003, **107**, 5483-5486.

- 15 Y. Nosaka, M. Matsushita, J. Nishino and A. Y. Nosaka, *Science and Technology of Advanced Materials*, 2005, **6**, 143-148.
- 16 M. Miyauchi, A. Ikezawa, H. Tobimatsu, H. Irie and K. Hashimoto, *Physical Chemistry Chemical Physics*, 2004, **6**, 865.
- 17 H. Kisch, L. Zang, C. Lange, W. F. Maier, C. Antonius and D. Meissner, *Angewandte Chemie International Edition*, 1998, **37**, 3034-3036.
- 18 Murdoch M, G. I. N. Waterhouse, M. A. Nadeem, J. B. Metson, M. A. Keane, R. F. Howe, Llorca J and Idriss H, *Nat Chem*, 2011, **3**, 489-492.
- 19 V. Subramanian, E. E. Wolf and P. V. Kamat, *Journal of the American Chemical Society*, 2004, **126**, 4943-4950.
- 20 S. Sato and J. M. White, *Chemical Physics Letters*, 1980, **72**, 83-86.
- 21 C. M. Wang, A. Heller and H. Gerischer, *Journal of the American Chemical Society*, 1992, **114**, 5230-5234.
- 22 T. Hirakawa and P. V. Kamat, *Journal of the American Chemical Society*, 2005, **127**, 3928-3934.
- 23 K. Maeda and K. Domen, *The Journal of Physical Chemistry Letters*, 2010, **1**, 2655-2661.
- 24 R. Abe, *Journal of Photochemistry and Photobiology C: Photochemistry Reviews*, 2010, **11**, 179-209.
- 25 H. Irie, S. Miura, K. Kamiya and K. Hashimoto, *Chemical Physics Letters*, 2008, **457**, 202-205.
- 26 H. Irie, K. Kamiya, T. Shibamura, S. Miura, D. A. Tryk, T. Yokoyama and K. Hashimoto, *The Journal of Physical Chemistry C*, 2009, **113**, 10761-10766.
- 27 H. Yu, H. Irie, Y. Shimodaira, Y. Hosogi, Y. Kuroda, M. Miyauchi and K. Hashimoto, *The Journal of Physical Chemistry C*, 2010, **114**, 16481-16487.
- 28 M. Liu, X. Qiu, M. Miyauchi and K. Hashimoto, *Chemistry of Materials*, 2011, **23**, 5282-5286.
- 29 M. Liu, X. Qiu, M. Miyauchi and K. Hashimoto, *Journal of the American Chemical Society*, 2013, **135**, 10064-10072.
- 30 M. Nishikawa, Y. Mitani and Y. Nosaka, *The Journal of Physical Chemistry C*, 2012, **116**, 14900-14907.
- 31 C. Creutz, B. S. Brunschwig and N. Sutin, *The Journal of Physical Chemistry B*, 2005, **109**, 10251-10260.
- 32 M. Liu, K. Sunada, K. Hashimoto and M. Miyauchi, *Journal of Materials Chemistry A*, 2015, **3**, 17312-17319.
- 33 M. Liu, X. Qiu, M. Miyauchi and K. Hashimoto, *Journal of the American Chemical Society*, 2013, **135**, 10064-10072.
- 34 M. Liu, R. Inde, M. Nishikawa, X. Qiu, D. Atarashi, E. Sakai, Y. Nosaka, K. Hashimoto and M. Miyauchi, *ACS Nano*, 2014, **8**, 7229-7238.
- 35 S. Brunauer, P. H. Emmett and E. Teller, *Journal of the American Chemical Society*, 1938, **60**, 309-319.
- 36 A. Kondo, G. Yin, N. Srinivasan, D. Atarashi, E. Sakai and M. Miyauchi, *Nanoscale*, 2015, **7**, 12510-12515.
- 37 Y. Ohko, D. A. Tryk, K. Hashimoto and A. Fujishima, *The Journal of Physical Chemistry B*, 1998, **102**, 2699-2704.
- 38 N. J. Huo, S. X. Yang, Z. M. Wei and J. B. Li, *J. Mater. Chem. C*, 2013, **1**, 3999-4007.
- 39 P. M. Kowalski, B. Meyer and D. Marx, *Physical Review B*, 2009, **79**, 115410.
- 40 M. Ramamoorthy, R. D. King-Smith and D. Vanderbilt, *Physical Review B*, 1994, **49**, 7709-7715.
- 41 Y. Hou, F. Zuo, A. P. Dagg, J. K. Liu and P. Y. Feng, *Adv. Mater.*, 2014, **26**, 5043-5049.
- 42 W. J. Li, P. M. Da, Y. Y. Zhang, Y. C. Wang, X. Lin, X. G. Gong and G. F. Zheng, *Acs Nano*, 2014, **8**, 11770-11777.
- 43 J. A. Seabold and K. S. Choi, *Chem. Mat.*, 2011, **23**, 1105-1112.
- 44 Z.-G. Zhao and M. Miyauchi, *Angewandte Chemie*, 2008, **120**, 7159-7163.
- 45 Y. Nosaka, S. Takahashi, H. Sakamoto and A. Y. Nosaka, *The Journal of Physical Chemistry C*, 2011, **115**, 21283-21290.
- 46 M. Miyauchi, A. Nakajima, K. Hashimoto and T. Watanabe, *Advanced materials*, 2000, **12**, 1923-1927.
- 47 M. Miyauchi, A. Nakajima, T. Watanabe and K. Hashimoto, *Chemistry of Materials*, 2002, **14**, 4714-4720.
- 48 A. Iwaszuk and M. Nolan, *Physical Chemistry Chemical Physics*, 2011, **13**, 4963-4973.
- 49 S. Anandan and M. Miyauchi, *Chemical communications*, 2012, **48**, 4323-4325.
- 50 R. Abe, H. Takami, N. Murakami and B. Ohtani, *Journal of the American Chemical Society*, 2008, **130**, 7780-7781.
- 51 T. Arai, M. Yanagida, Y. Konishi, Y. Iwasaki, H. Sugihara and K. Sayama, *Catalysis Communications*, 2008, **9**, 1254-1258.
- 52 M. Shibuya and M. Miyauchi, *Advanced materials*, 2009, **21**, 1373-1376.

Ti(IV) clusters act accelerate photocatalytic oxidation of organic compounds.

